

Preparation of mesoporous CaO-ZrO₂ catalysts without template for the continuous synthesis of glycerol carbonate in a fixed-bed reactor

Xuelan Zhang^{a,*}, Shuwei Wei^a, Xueying Zhao^a, Zheng Chen^a, Hongwei Wu^a, Ping Rong^a, Yu Sun^a, Ya Li^a, Hao Yu^b, Dengfeng Wang^{a,*}

^a College of Chemistry, Chemical Engineering and Materials Science, Zaozhuang University, Zaozhuang, 277160, China

^b College of Chemical and Environmental Engineering, Shandong University of Science and Technology, 266590, Qingdao, China

ARTICLE INFO

Keywords:

Glycerol
Glycerol carbonate
CaO-ZrO₂
Fixed-bed

ABSTRACT

Recently, transformation of glycerol into glycerol carbonate (GLC) has been of critical importance. Although traditional Ca-based catalysts present high activity for the GLC synthesis, their industrial applications are hindered by the leaching of Ca²⁺. Here, a series of mesoporous CaO-ZrO₂ with high surface area were obtained without template. CO₂ temperature-programmed desorption displayed that the basic properties of the catalysts can be controlled by the content of Ca dopant. Importantly, Ca²⁺ can be introduced into *t*-ZrO₂ lattice, resulting in the formation of a solid solution structure. Based on systematic experiments, a correlation between their basic properties and catalytic behavior was explained. Under the optimized conditions, the catalyst with a certain ratio of Ca: Zr = 0.6: 1 showed an excellent performance with a 97% glycerol conversion and a 93% selectivity of GLC. Furthermore, the solid solution structure rendered this catalyst high resistance to reactant flushing in a fixed-bed, without leaching of active sites.

1. Introduction

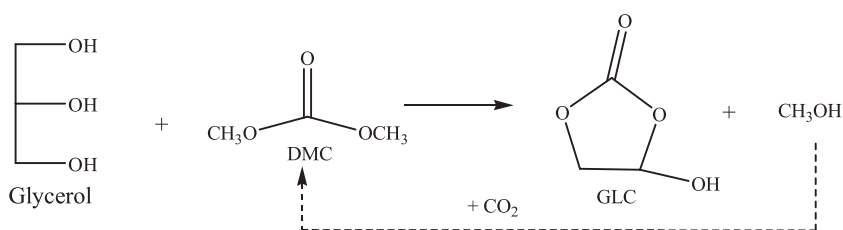
In the past decades, special attention has been paid to biodiesel production owing to depletion of fossil energy and to environmental problems. As an important renewable energy, the utilization of biodiesel not only solves the issue of energy-crisis, but also generates little negative effects on the ecosystem [1]. Considering these aspects, its production scale would be expanded rapidly in a short time. However, we are meeting a tremendous challenge that a great deal of glycerol (about 100 g/kg of biodiesel) is created as an undesired product. Consequently, a surplus waste of glycerol would reduce the market competitiveness of biodiesel industry, and therefore, it is an urgent need to convert glycerol into chemicals of high-added value [2]. Among the kinds of glycerol derivatives, glycerol carbonate (GLC) has been attracted much attention due to its outstanding physic-chemical features including non-toxicity, low-flammability, high biodegradability and water-solubility [3,4]. Moreover, it has been reported that GLC is a chief raw material to produce other fine chemicals such as adhesive, surfactant, polymers and elastomer. In addition, GLC is also a green solvent with high polarity, so it has been applied broadly in paint and electrochemistry fields [3–6]{Ochoa-Gómez, 2012 #3;Sonnati, 2013 #4}. Conventionally, GLC was prepared from the reaction between

glycerol and phosgene or CO, which had been obsoleted due to their high-toxic and unsafe properties of phosgene or CO [7,8]. The preparation of GLC from CO₂ and glycerol has been studied extensively and is still a current interest. However, this approach only gives a minimal GLC yield but requires harsh reaction conditions, inhibiting its further practical employment [9–11]. To solve this problem, urea, which is regarded as an activated form of CO₂, has been applied to the synthesis of GLC and its analogues [6,12–14]. Although a relatively high yield of GLC could be achieved, the synthesis of GLC from urea and glycerol must be conducted at low pressures below 20–30 mbar in order to remove the gaseous ammonia. In addition, the GLC selectivity is often far from satisfactory because of undesired side-reactions. Compared to aforementioned processes, the synthesis of GLC via transesterification between glycerol and dimethyl carbonate (DMC) is more promising and facile [15–17]. Meanwhile, the co-product methanol can be easily separated because of its low boiling point (around 64.7 °C). More interestingly, DMC could be synthesized directly from CO₂ and methanol, which is the by-product generated in the process, making the entire cycle efficient and sustainable (cf. Scheme 1) [18,19].

Recently, Tudorache et al. prepared an expensive enzymatic catalyst for the reaction of DMC and glycerol, but this catalytic system was highly sensitive to poisoning. Worse still, a relative long reaction time

* Corresponding authors.

E-mail addresses: mhszxl@sxicc.ac.cn (X. Zhang), bitwdf@163.com (D. Wang).



Scheme 1. Synthesis of GLC via transesterification between glycerol and DMC: indirect utilization of CO₂.

was required to achieve good catalytic performance [20]. It is well accepted that basic catalysts exhibit superior catalytic ability over acidic samples towards GLC synthesis. Homogeneous basic catalytic samples like NaOH and K₂CO₃ could promote GLC synthesis efficiently, but they suffered from the inconvenience of separating catalysts and products [21]. With the aim of avoiding this disadvantage, several heterogeneous basic materials have been explored. For instance, basic catalysts containing alkali metal elements like NaOH/ γ -Al₂O₃ [22], K₂CO₃/MgO [22], KF/ γ -Al₂O₃ [23], Li/ZnO [24] and Na-modified zeolite [25] have been used for the GLC formation. Unfortunately, some basic species from these catalysts would be leaching into the reaction systems, leading to a poor catalytic stability. Diverse mixed oxides such as ZnO/La₂O₃ [26], MgO/La₂O₃ [27], Mg/Zr/Sr mixed oxides [28] and fluorine-doped Mg/Al mixed oxides [29] were also evaluated. Despite their high reactivity, the GLC selectivity was often suppressed owing to severe side-reactions.

In addition to these basic materials mentioned above, the Ca-based samples have attracted a broadly attention. Ochoa-Gómez et al. found that CaO possessed the highest activity among several alkali earth metal oxides [21]. However, CaO was easily poisoned and deactivated by water and carbon dioxide. Later, Li concluded that the catalytic ability of CaO originated from the homogeneous Ca-species, which was generated due to its interaction with DMC and glycerol [30]. This conclusion was also ascertained by Simanjuntak and his co-workers [31]. Zheng et al. disclosed that Ca-Al-O hydrocalumite could give a 93% conversion of glycerol. Meanwhile, Ca/Al mixed oxides derived this precursor were also active for the GLC production [32]. Besides, Granados-Reyes et al. suggested that Ca/Al layered double hydroxide could be applied to catalyze the GLC manufacture [33]. In addition, CaO-MgO was also selected as a catalyst [34]. Nevertheless, further investigations revealed that the active CaO phase could dissolve into the reacting glycerol, generating a calcium glycerol species [31,32]. Even worse, traditional Ca-based catalysts suffered from limited specific area, lowering their reactivity to a certain degree [32]. Thus, the development a Ca-based solid basic catalyst with high activity and stability for the GLC synthesis from glycerol and DMC is still highly desirable and remains as a great challenge.

On the other hand, zirconia was regarded as a promising catalytic promoter and supporter for numerous base-catalyzed organic reactions, benefiting from the distinct thermal stability and high surface area of zirconia [35]. Many researchers have proved that an insertion of alkali metal ions and alkaline earth ions into zirconia could enhance both surficial basicity and structural stability of the resulting catalyst, which in turn promotes their catalytic activity and reusability significantly. For instance, mesoporous Na₂O-ZrO₂ basic catalysts were acquired for the efficient manufacture of DMC and propylene glycol [36]. Liu et al. and Varkolu et al. found that mesoporous MgO-ZrO₂ could promote the production of propylene glycol methyl ether and glycerol carbonate with high reactivity, respectively [37,38]. In their approaches, organic zirconium (IV) and pluronic P123 were chosen as a starting material and a template respectively to obtain a mesoporous framework. Undoubtedly, this brought about a high cost by this type of catalysts [36–38]. Coupled with the weakness that these catalysts were prepared via a complicated sol-gel procedure, a more cheap and convenient method should be established. Actually, we have prepared mesoporous MgO-ZrO₂ catalysts via simple co-precipitation method using zirconium

nitrate as Zr source [39]. Nevertheless, few studies investigated the preparation of CaO-ZrO₂ samples via a similar manner. Meanwhile, the effect of Ca²⁺ ion doping on zirconia and the catalytic performance of the CaO-ZrO₂ catalysts in the continuous GLC synthesis are remained unknown.

In the present work, a series of mesoporous CaO-ZrO₂ catalysts with different contents of calcium were prepared via a co-precipitation procedure which is free of a template. The physicochemical properties of the prepared catalysts were characterized by XRD, BET, Raman, XPS, TEM and by the CO₂ temperature-programmed desorption (CO₂-TPD) measurements. Aim at obtaining a stable Ca-modified solid base system, we will demonstrate that these catalysts are particularly efficient for the continuous GLC synthesis in a fixed-bed reactor, and moreover Ca species are not leaching anymore.

2. Experimental

2.1. Preparation of catalysts

CaO-ZrO₂ catalytic samples were synthesized via a co-precipitation using metal nitrates as starting materials. Briefly, a CaO-ZrO₂ (0.6:1) catalyst was used as an example to demonstrate the preparation process: 0.7 g Ca(NO₃)₂·4H₂O (3 mmol) and 2.15 g Zr(NO₃)₄·5H₂O (5 mmol) were dissolved into 50 mL deionized water under stirring until completely dissolved. Meanwhile, 1.04 g NaOH (26 mmol) was dissolved into another 50 mL deionized water as precipitant. Subsequently, the two solutions were slowly added into a 500 mL beaker under vigorous stirring with pH of 10.0. After the titration, the suspension was stirred for 2 h at room temperature. Then, the precipitate was washed with an excess of deionized water to remove Na⁺ ions. The filter cake was refluxed in deionized water at 80 °C for 48 h. Once the slurry cooled down to room temperature, the solid products were collected and then dried at 80 °C for 12 h. Finally, the dried products were calcined at 600 °C for 7 h under a flowing steam of nitrogen. For convenience, the mixed oxide catalysts were designated as *n*CaO-ZrO₂, where *n* presented the starting Ca²⁺:Zr⁴⁺ atomic ratio in the mother solution (*n* = 0, 0.2, 0.4, 0.6 or 0.8). For a comparison, pure ZrO₂ was also prepared in the similar manner without adding Ca (NO₃)₂·4H₂O in the starting mixture.

2.2. Samples characterization

Structural characterization of the catalysts was carried out on a Rigaku Miniflex diffractometer with Ni-filtered Cu K α radiation using a step of 5°/min (in a 2 θ range of 0–8° for low-angle XRD patterns and 10–80° for wide-angle XRD patterns).

X-ray photoelectron spectroscopy (XPS) experiments were performed by a Thermo Scientific k-Alpha spectrometer with Al K α (1486.6 eV) radiation. The binding energy of the adventitious carbon (C 1s) was set at 284.6 eV for correction. Prior to the measurements, all the samples were treated under vacuum for 3 h.

The Raman spectra were recorded on a Horiba-Jobin-Yvon spectrometer equipped with a He-Ne laser light source excited by a wavelength of 632.8 nm.

The textural properties including surface area (BET), pore volume and pore size distribution of the catalysts were derived from N₂

adsorption-desorption technique using a Micromeritics ASAP-2020 instrument at $-196\text{ }^{\circ}\text{C}$. Prior to the collection of adsorption isotherms, catalysts were pretreated in vacuum at $300\text{ }^{\circ}\text{C}$ for 5 h.

In order to determine the elemental composition, an inductively coupled plasma-optical (ICP) emission spectroscopy (PerkinElmer ICP OPTIMA-3000) was applied.

High resolution transmission electron microscopic (TEM) images were observed on a transmission electron microscope (FEI Tecnai F20) with a field emission gun at 200 kV.

CO_2 -TPD experiments were employed to study the basic properties of the catalysts. Firstly, the sample (0.20 g) was put in a quartz reactor bed and pre-treated in a flow of Ar (40 mL min^{-1}) at $600\text{ }^{\circ}\text{C}$ for 2 h, and then decreased to $30\text{ }^{\circ}\text{C}$. After the absorption of CO_2 (40 mL min^{-1}) for 2 h using a six-way valve, the catalyst was swept with Ar (40 mL min^{-1}) for 3 h to eliminate all physisorbed CO_2 at surface. Finally, the CO_2 -TPD experiment was carried out between $30\text{--}700\text{ }^{\circ}\text{C}$ with a heating rate of $10\text{ }^{\circ}\text{C min}^{-1}$ and the desorbed CO_2 was measured using an on-line gas chromatography (GC) with a TCD detector.

2.3. Catalytic reaction

In order to investigate the catalyst life more practically, the transesterification of DMC and glycerol was carried out in a continuous-flow, vertical stainless fixed-bed tubular reactor (8 mm inner diameter, 600 mm length) equipped with a stuff vessel of 300 mL, a product condenser and a product vessel of 3000 mL. The reactor was heated by a furnace with a thermocouple and a temperature controller. Typically, a 3-mL catalyst (2.6 g, 40–60 mesh) was placed in the thermostatic zone of the reactor. After the catalyst was heated to the desired temperature in a short time, the reactant mixture of DMC and glycerol (n (DMC): n (glycerol) = 3:1) was continuously fed into the reactor using a Gilson pump. The reaction products were cooled in the product condenser. Once all the parameters remained unchanged, a regular sampling was collected for quantitative analysis by a GC equipped with a HP-5 capillary column and a flame ionization detector. The column temperature ramp was: $70\text{ }^{\circ}\text{C}$ for 3 min, then heating up to $240\text{ }^{\circ}\text{C}$ at $30\text{ }^{\circ}\text{C min}^{-1}$, and $240\text{ }^{\circ}\text{C}$ for 4 min. The products were identified by a GC-MS (Agilent 7890-700B) with HP-5MS capillary column (30 m). Glycerol conversion (X_{glycerol}), GLC selectivity (S_{GLC}) were calculated by the following expressions. GLC yields (Y_{GLC}) were determined by multiplying conversion and selectivity.

$$X_{\text{glycerol}} = \frac{\text{moles of initial glycerol} - \text{moles of final glycerol}}{\text{moles of initial glycerol}} \times 100\%$$

$$S_{\text{GLC}} = \frac{\text{moles of GLC formed}}{\text{moles of initial glycerol} - \text{moles of final glycerol}} \times 100\%$$

$$Y_{\text{GLC}} = X_{\text{glycerol}} \times S_{\text{GLC}} \times 100\%$$

To better understand the correlation between the number of basic sites and glycerol conversion, the turnover frequencies (TOF) were determined by the following principle:

$$\text{TOF} = \frac{10^4 \times X_{\text{glycerol}} \times \text{LHSV}}{(M_{\text{glycerol}} + 3 \times M_{\text{DMC}}) \times T_B}$$

in which, LHSV is liquid hourly space velocity (h^{-1}); M_{glycerol} and M_{DMC} are molecular weight of glycerol and DMC, respectively (g mol^{-1}); T_B is the total number of basic sites present on the catalysts ($\mu\text{mol g}^{-1}$).

3. Results and discussion

3.1. Textual and structural properties of the prepared samples

The wide-angle XRD patterns of CaO-ZrO_2 solid bases are shown in Fig. 1(a). In this work, pure ZrO_2 was observed in a mixture of monoclinic and tetragonal phases. Specifically, the peaks at 23.9° , 28.1° and

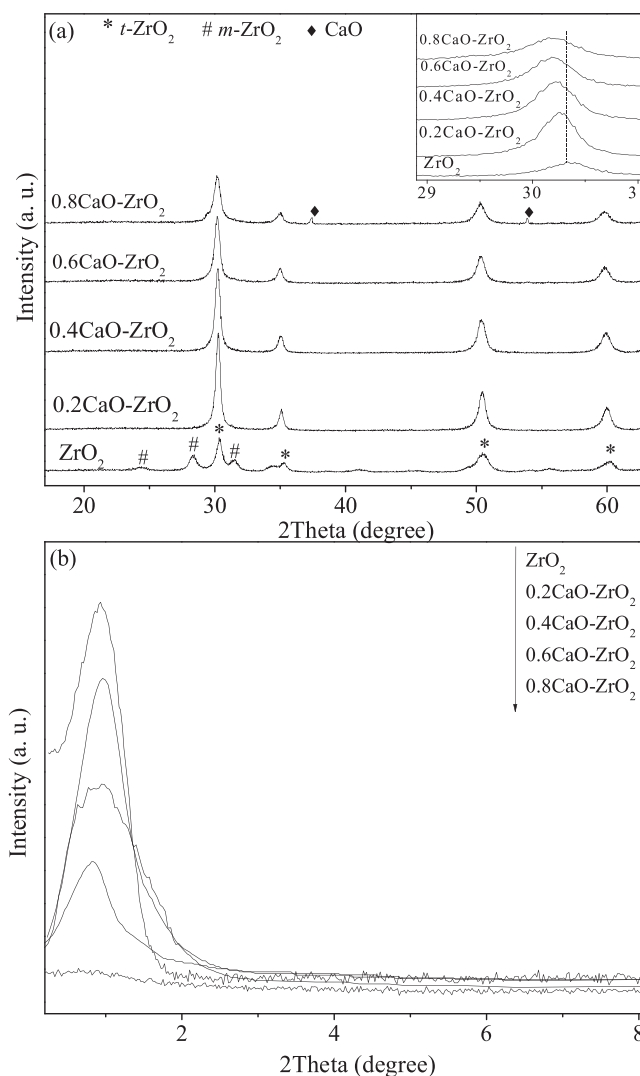


Fig. 1. XRD patterns of $n\text{CaO-ZrO}_2$ catalysts: (a), wide angle; (b), low angle.

31.4° were related to monoclinic ZrO_2 ($m\text{-ZrO}_2$ JCPDS No. 37-1484), and tetragonal ZrO_2 ($t\text{-ZrO}_2$, JCPDS No. 50-1089) was detected at 30.2° , 34.9° , 50.3° and 59.6° . This differed from the result reported by Wang et al., who found that $m\text{-ZrO}_2$ phase was mainly found for ZrO_2 using $(\text{NH}_4)_2\text{CO}_3$ as precipitant [40]. In this study, we selected NaOH to synthesize the catalyst precursors, and thus the anion on the surface of such samples would be partly neutralized by Na^+ ion during aging. This conferred precursors to have a tetragonal structure, and in turn benefiting for the creation of $t\text{-ZrO}_2$ in the final catalysts [41]. Upon the addition of Ca^{2+} , the peaks to $m\text{-ZrO}_2$ disappeared and all the mixed oxides only retained $t\text{-ZrO}_2$. This finding was attributed to the fact that the crystal structure of $t\text{-ZrO}_2$ could be stabilized selectively after the insertion of foreign atoms [36–38]. Herein, benefiting from the doping of Ca^{2+} , the structure of $t\text{-ZrO}_2$ was extremely stable even after thermal treatment at $600\text{ }^{\circ}\text{C}$. Importantly, it should be noted that the diffraction reflection related to calcium oxide was not observed when n was less than 0.8. Meanwhile, the peak assigned to $t\text{-ZrO}_2$ at about 30.2° continuously moved from higher to lower 2θ values with the rise of n , being in good agreement with those reported by Pradhan et al. [42]. Apart from this, the intensity of characteristic peaks assigned to $t\text{-ZrO}_2$ became weaker and weaker. Furthermore, the data listed in Table 1 demonstrated that the lattice parameters based on this peak expanded gradually because the ionic radius of Ca^{2+} (1.0 \AA) was longer than that of Zr^{4+} (0.84 \AA) [42]. Therefore, all these obtained results excluded the possibility of generation of amorphous form of CaO for samples with n

Table 1
Textural chemical and basic properties of various CaO-ZrO₂ catalysts.

Sample	Ca ²⁺ :Zr ⁴⁺ atomic ratio		d_{XRD} (Å) ^c	S_{BET} (m ² g ⁻¹)	Pore volume (cm ³ g ⁻¹)	Average pore diameter (nm)	Number of basic sites (μmol g ⁻¹) and contribution ^d			
	Initial ^a	In solid ^b					Total	W.	M.	S.
ZrO ₂	–	–	2.9453	252	0.28	4.6	43	18.3 (42.6)	21.7 (50.4)	3.0 (7.0)
0.2CaO-ZrO ₂	0.2: 1	0.08:1	2.9511	243	0.33	5.4	88	37.4 (42.5)	40.6 (46.1)	10.0 (11.4)
0.4CaO-ZrO ₂	0.4: 1	0.36:1	2.9513	212	0.37	8.3	113	35.8 (31.7)	51.5 (45.6)	25.7 (22.7)
0.6CaO-ZrO ₂	0.6: 1	0.55:1	2.9587	167	0.32	9.2	138	36.1 (26.1)	63.6 (46.1)	38.3 (27.8)
0.8CaO-ZrO ₂	0.8: 1	0.73:1	2.9607	87	0.49	10.1	104	34.3 (33.0)	34.1 (32.8)	35.6 (34.2)

^a The nominal atomic ratio in the mother solution.

^b Measured by ICP for the final solid catalysts.

^c Based on the XRD peak at 30.2°.

^d The value in parentheses is the contribution of single basic sites to the total number of total basic sites. W.: Weak sites; M.: Medium basic sites; S.: strong basic sites.

from 0.2 to 0.6. In light of the fact that the divalent alkali-earth metal ions could substitute Zr⁴⁺ in the host lattice to generate a stable solid solution, the absence of separated CaO peak could be explained by the formation of CaO-ZrO₂ solid solution when n was varied from 0.2 to 0.6 [37–39]. Nevertheless, due to the limited capacity of ZrO₂ for incorporating CaO dissolution into its lattice, two featured diffraction peaks assigned to CaO were observed (JCPDS No. 48-1467) at 37.3° and 53.8° as n was further increased to 0.8. Noting that the width of peaks became smaller after insertion of Ca²⁺, the average crystallite sizes were thus calculated based on 2θ of 30.2° by the Scherrer formula. The crystallite sizes of ZrO₂, 0.2CaO-ZrO₂, 0.5CaO-ZrO₂, 0.6CaO-ZrO₂, and 0.8CaO-ZrO₂ were 12.8, 16.9, 15.5, 14.8 and 11.5 nm, respectively. At the same time, the following TEM measurement further affirmed that these samples consisted mainly of crystals with a size of 5–20 nm, suggesting that they were a class of nano-catalysts. Fig. 1(b) gives the low-angle XRD patterns of n CaO-ZrO₂ catalysts. It could be seen that all the catalysts show a sharp and symmetric peak at about $2\theta = 1^\circ$, which was corresponding to their mesoporous structure [39]. As discussed above, the addition of excessive Ca²⁺ into the system induced the appearance of free CaO phase, which was adverse to the generation of a uniformly mesoporous framework. As a result, ZrO₂ exhibited the highest intensity of diffraction, whereas Ca-rich sample (0.8CaO-ZrO₂) presented the lowest one. This is consistent with the results of these kinds of Zr-based solid bases in previous literature [37,39].

It was accepted that Raman analysis was an effective technique to study the microstructure of Zr-containing materials. Raman spectra of n CaO-ZrO₂, pure ZrO₂ and CaO are shown in Fig. 2. Apparently, bare ZrO₂ support presented not only the characteristic peaks of t -ZrO₂ at 269, 314, 460 and 645 cm⁻¹, but also the typical reflections to monoclinic ZrO₂ phase at 331, 380, 536 and 559 cm⁻¹ [40,42]. This fact is in line with its XRD result in Fig. 1(a). In contrast, samples of 0.2CaO-ZrO₂, 0.4CaO-ZrO₂ and 0.6CaO-ZrO₂ demonstrated the peaks attributed to t -ZrO₂ only. No Raman lines due to m -ZrO₂ or CaO were detected. These also suggested that doping a foreign Ca atom could convert ZrO₂ from a monoclinic to a tetragonal phase. In addition, it should be noted that the peaks of these Ca-modified samples widened obviously, due to the existence of oxygen vacancy which was resulted from the incorporation of Ca²⁺ into the ZrO₂ lattice [43,44]. Furthermore, the peaks at 269 and 645 cm⁻¹ had a slight shift to lower wavenumbers for mixed oxide catalysts with a rise of Ca content, further affirming that they possessed a stable structure of CaO-ZrO₂ solid solution. Nevertheless, a new reflection corresponding to CaO emerged at 289 cm⁻¹ for 0.8CaO-ZrO₂ sample due to that some free CaO particles were formed on its surface (see Fig. 1(a)).

To further verify the generation of CaO-ZrO₂ solid solution, all the samples were analyzed in-depth by the XPS measurements. For pure ZrO₂, its C 1s spectra gave an intense reflection at 284.5 eV and a shoulder peak at 289.1 eV (see Fig. 3(a)). The former one was attributed to the adventitious carbon, while the latter one was originated from the

minor carbonate species [45]. As illustrated by the following CO₂-TPD characterization, their basic strength was determined by the amount of Ca content. Considering that a stronger basic strength would result in the formation of carbonate species with a higher stability, and thus, the catalyst 0.8CaO-ZrO₂ showed the most intense peak at 289.5 eV, owing to its superior basic strength than other samples. Apart from this, the gradual rise of binding energy from 289.1 to 289.5 eV with a rise of n also pointed the incorporation of Ca²⁺ into ZrO₂ lattice. The typical Zr 3d spectra are presented in Fig. 3 (b). For pristine ZrO₂, there appeared two peaks at 184.2 and 181.8 eV with a high intensity, which were associated with Zr 3d_{5/2} and Zr 3d_{3/2} energy states of Zr(IV) oxide species, respectively [46]. The intensity of these two reflections gradually decreased with an increase of Ca content. Meanwhile, it is worth noting that adding Ca into ZrO₂ support could give rise to a continue increase of Zr 3d binding energy. These observations also support that Ca²⁺ had entered into the t -ZrO₂ lattice, creating a solid solution. Fig. 3(c) displays the Ca 2p spectra of these catalysts, and the XPS spectrum of single CaO is also presented for a comparison. When $n < 0.8$, all the catalysts exhibited a broad and intense band centered at 346.1 eV related to the emission from Ca 2p_{3/2} of Ca²⁺ in oxide state [46,47]. In the case of sample 0.8CaO-ZrO₂, its spectral profile was similar to that of CaO, in which an additional peak was observed at about 350.5 eV. According to the previous work, this satellite peak can be assigned to Ca 2p_{1/2} state of Ca²⁺ [46,47]. More importantly, the binding energies of Ca 2p_{2/3} in all the mixed oxides were lower than that of pure CaO, because the n CaO-ZrO₂-containing materials possessed a solid solution structure. Fig. 3(d) depicts the O1s spectra of these materials. For samples ZrO₂, 0.2CaO-ZrO₂, 0.4CaO-ZrO₂ and 0.6CaO-ZrO₂, the Ca content did not influence the shape of the O1s curves largely. Precisely, only a sharp peak appeared at about 529.7 eV. According to Pradhan et al., this peak was ascribed to the lattice oxygen of the CaO-ZrO₂ solid solution [42]. Moreover, the appearance of this O1s peak also implied that strong Lewis basic sites were present at their surfaces [6], being in line with the following CO₂-TPD characterization results. As to the Ca-rich sample (0.8CaO-ZrO₂), beside this peak, a new one with a mild intensity emerged at 531.2 eV, which was consistent with the O1s spectrum of pure CaO [48]. This result can be explained as follows: all the Ca²⁺ ions were introduced into t -ZrO₂ lattice without creation of any free CaO when $n < 0.8$, and thus only the O1s peak related to the lattice oxygen appeared. The catalyst 0.8CaO-ZrO₂ also had a counterpart of CaO oxygen due to the existence of separated CaO, judging from the XRD results. Thus, these two O1s reflections were clearly detected. At the same time, this also provided a strong support for the conclusion that CaO-ZrO₂ was in a solid solution state for samples of $0.2 \leq n \leq 0.8$. Additionally, in the case of Ca concentration for these mixed oxide samples, the measured XPS values were higher than those from the ICP measurements, implying that their surface was enriched in Ca (see Fig. S1 in Supplementary Material).

Textural properties of the n CaO-ZrO₂ catalysts are evaluated by an

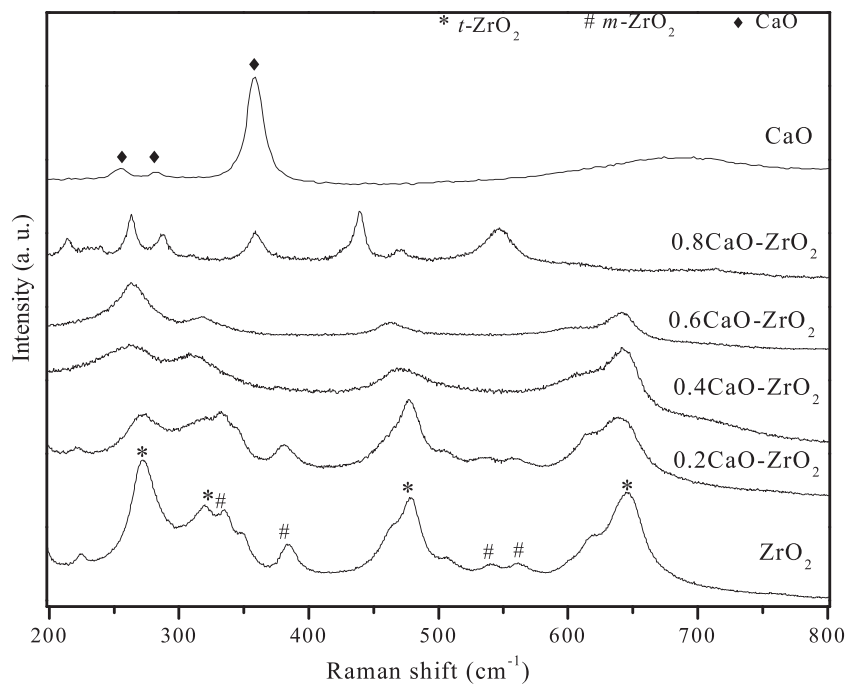


Fig. 2. Raman spectra of CaO, ZrO₂ and *n*CaO-ZrO₂ mixed oxides.

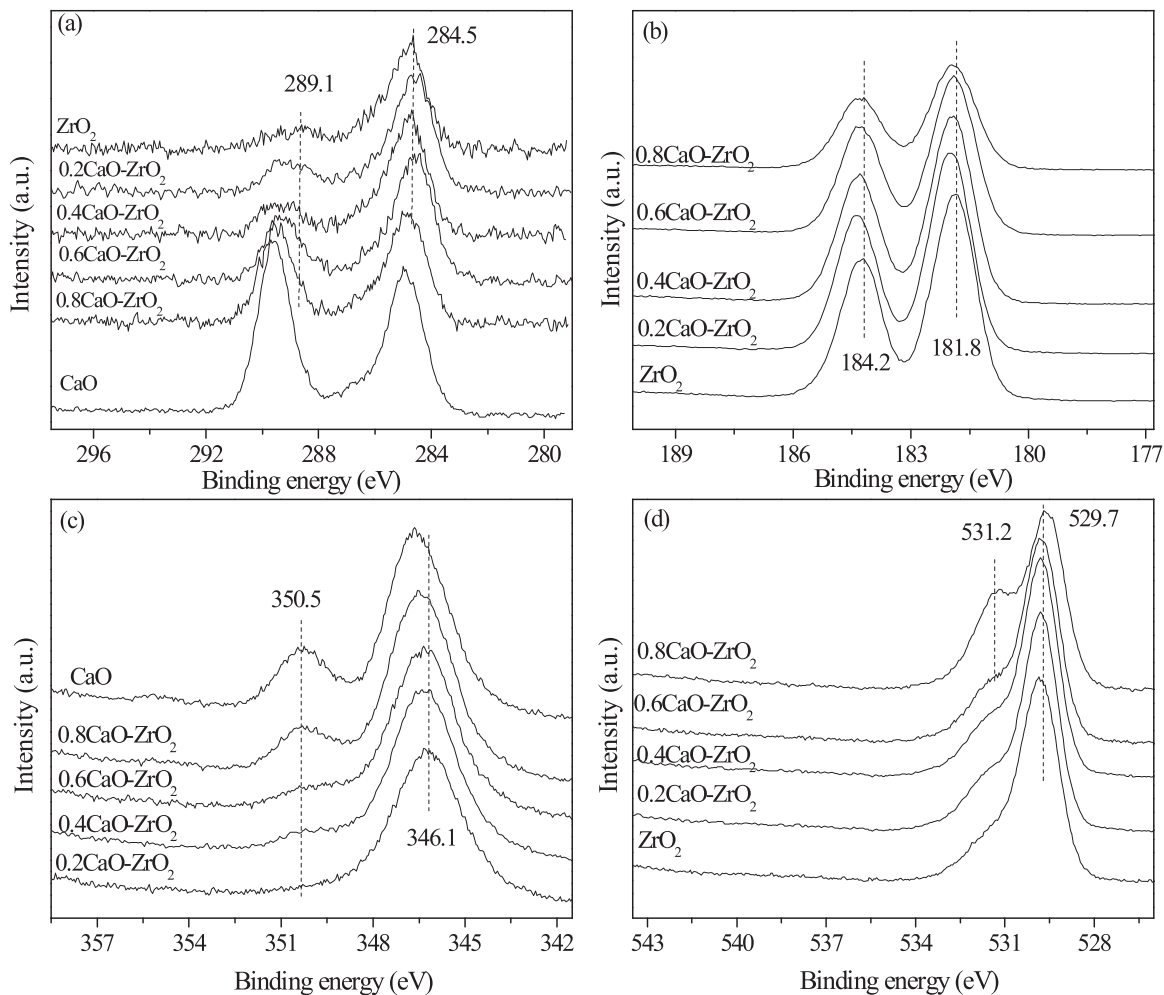


Fig. 3. C 1s (a), Zr 3d (b), Ca 2p (c) and O 1s (d) XPS spectra of CaO, ZrO₂ and *n*CaO-ZrO₂ samples.

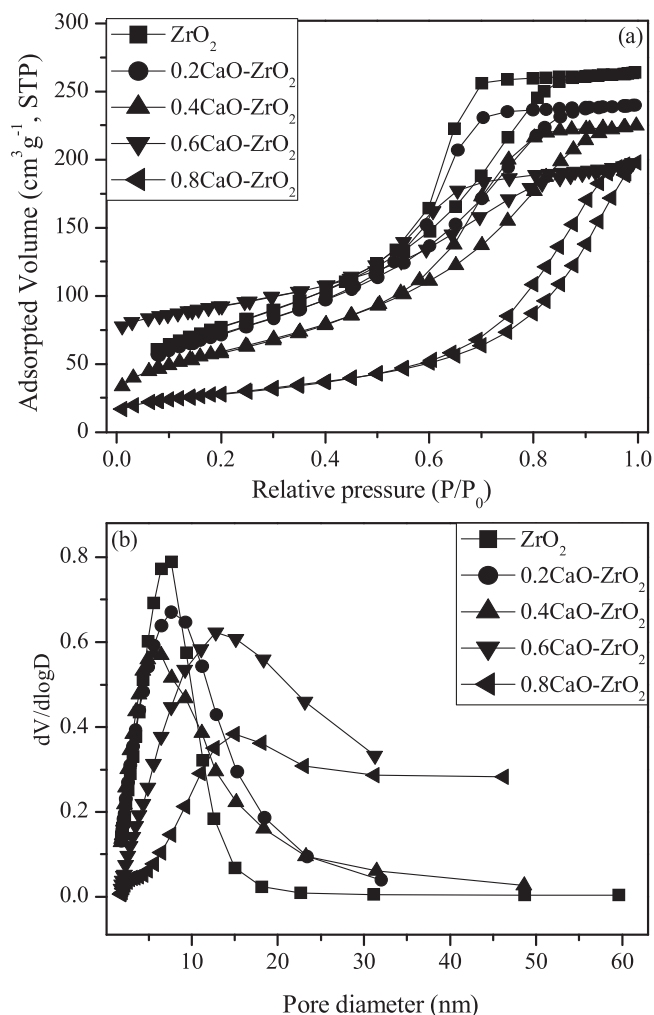


Fig. 4. N₂ adsorption-desorption isotherms (a) and pore-size distributions (b) of $n\text{CaO-ZrO}_2$ catalysts.

N₂ adsorption-desorption technique and the N₂ adsorption-desorption isotherms are displayed in Fig. 4. Apparently, all the isotherms were of type IV with clear hysteresis loops at higher relative pressure. Following the IUPAC principle, these catalytic materials were of mesoporous solid catalysts [49,50]. Moreover, it was notable that their hysteresis loops were greatly affected by the Ca content. For the pure ZrO₂ and Ca-poor samples (0.2CaO-ZrO₂ and 0.4 CaO-ZrO₂), hysteresis loops demonstrated an H2 type with $P/P_0 = 0.5-0.9$, suggesting the formation of an ordered structure of mesoporous [51]. In the case of the Ca-rich sample (0.8CaO-ZrO₂), H3 shaped hysteresis loops ($P/P_0 = 0.7-1.0$) were observed, indicating an existence of slit-shaped pores [51]. For 0.6CaO-ZrO₂, although it mainly presented H2 shaped hysteresis loops, the higher opening and closing P/P_0 position resembled that of H3 type. Collectively, all the above results indicate that an increase of Ca content makes their mesoporous structure unordered, which is also confirmed by the results in Fig. 1(b). The pore size distributions of the $n\text{CaO-ZrO}_2$ catalysts are also given in Fig. 4(b). It could be found that all the samples exhibited substantially developed porous structures, and their pore sizes were widely distributed between 5–50 nm. Moreover, the catalysts ZrO₂ and 0.2CaO-ZrO₂ presented a sharp pore volume distribution in a narrow and smaller pore diameter range, while a broad distribution peak of porous structure with a large pore diameter was observed for the catalytic materials with a high Ca content. This corroborated again that an excessive Ca amount did not facilitate formation of mesoporous structure. From the results reported in Table 1, it could be observed that the surface areas of these samples were significantly high, which was beneficial for them exposing more active sites. Simultaneously, the obtained data revealed that a decrease in surface area with an increasing n was ascribed mainly to the negative effect of a high Ca content on their mesoporous frameworks. Moreover, the pore diameters of the catalysts increased with a rise of the n value; clearly, the sample of 0.8CaO-ZrO₂ possessed the largest pore diameter.

TEM images of catalysts are shown in Fig. 5. All the samples except for 0.8CaO-ZrO₂ are composed mainly of nano-crystals with diameters of 10–20 nm, clustering together to generate a sponge-like network. In particular, the 0.6CaO-ZrO₂ catalyst had a continuous pore/channel with a 4–10-nm width. Interestingly, amorphous structures were dominant without appearance of obvious crystalline phase for this catalyst. However, some separated particles were detected for 0.8CaO-ZrO₂, which might be owing to the existence of free CaO particle at its

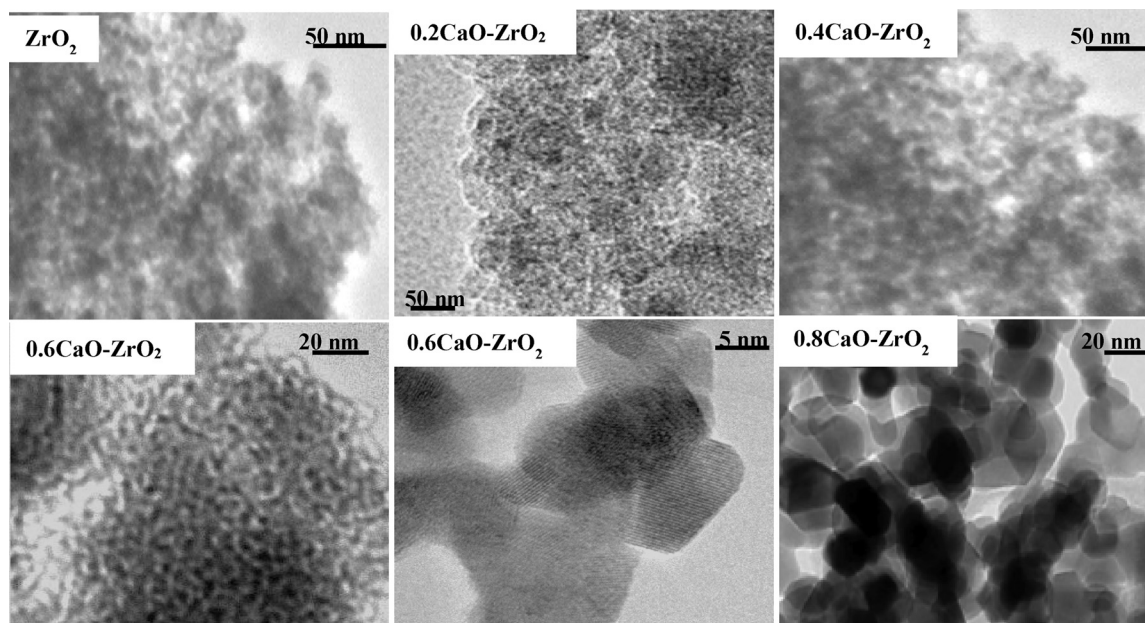


Fig. 5. TEM images of various $n\text{CaO-ZrO}_2$ catalysts.

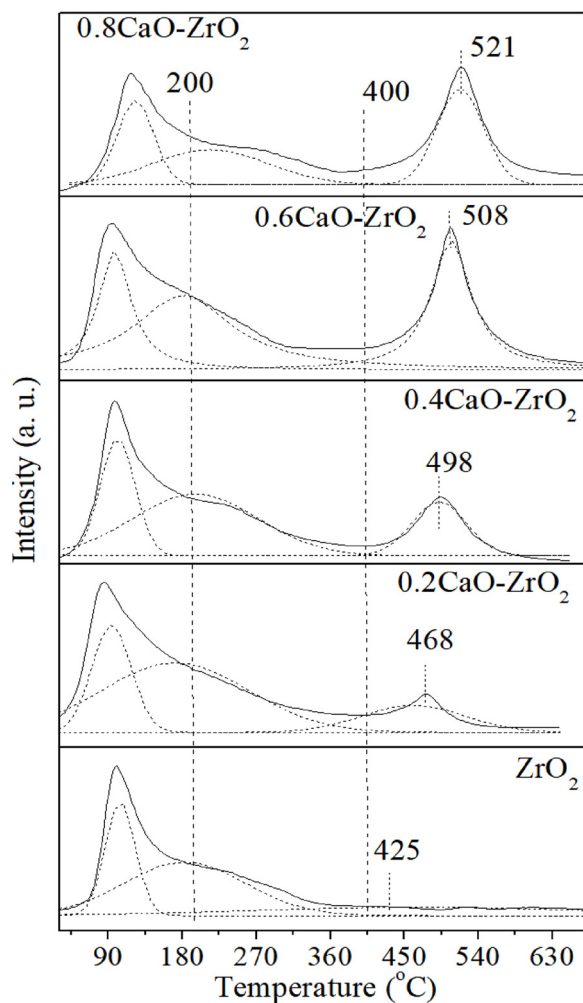


Fig. 6. CO₂-TPD of *n*CaO-ZrO₂ and ZrO₂ catalysts.

surface.

3.2. Surface basic properties

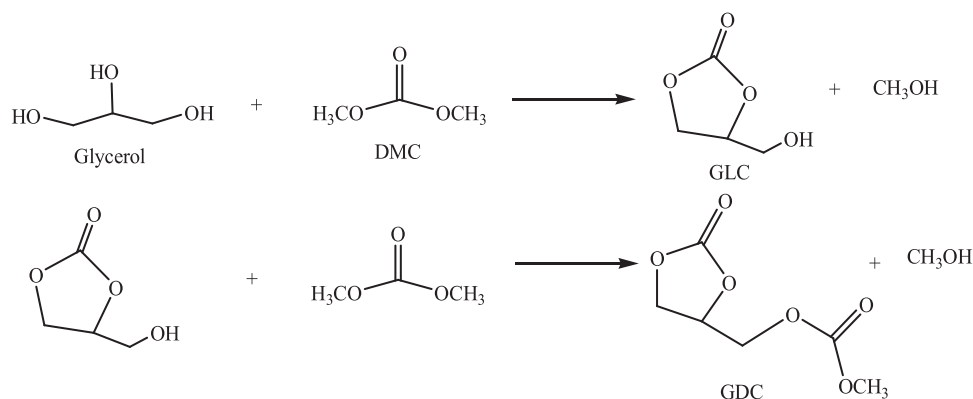
The basic properties of the *n*CaO-ZrO₂ catalysts were investigated using the CO₂-TPD measurement, and the CO₂ desorption curves are shown in Fig. 6. Generally speaking, the temperature for desorption peak was served to determine the basic species, and the basic strength could be reflected by the maximum desorption temperature. The amount of desorpted CO₂, corresponding to the peak area, was applied

to measure the catalyst basicity. Clearly, all the profiles in Fig. 6 consisted of three Gaussian peaks, which stood for weak basic sites (below 200 °C) and were attributed to OH⁻ groups, for moderate basic sites (between 200 and 400 °C) related to metal-oxygen pairs (including Ca-O and Zr-O), and for strong basic sites (over 400 °C) associated with an isolated O²⁻, respectively [39]. As expected, the strong basic sites of these samples shifted gradually towards higher orientations with a rise of *n*, illustrating that the introduction of Ca²⁺ could promote the basic strength of the resulted *n*CaO-ZrO₂ catalysts. In terms of basic strength, these catalysts gave a decreasing order of ZrO₂ < 0.2CaO-ZrO₂ < 0.4CaO-ZrO₂ < 0.6CaO-ZrO₂ < 0.8CaO-ZrO₂. Meanwhile, the basic site distributions were calculated and are summarized in Table 1 for all the catalysts. No doubt, the distributions of these samples varied greatly depending on the *n* value. Particularly, the strong basic peaks became more and more intense with a rise of *n*, at expense of weak and moderate basic sites belonging to ZrO₂. Consequently, the percentage of strong basic sites for 0.6CaO-ZrO₂ was 27.8%, which was about 4 times that of Ca-free sample (ZrO₂). The total number of basic sites increased sharply with an increasing of the Ca content when *n* ≤ 0.8, and then decreased with a further increase of *n*. This trend was caused by the double-edged effect of Ca²⁺ on the surface basicity. On the one hand, the amount of metal-oxygen (Ca-O) would increase with the addition of Ca²⁺, resulting in an improvement of the number of moderate basic sites. Simultaneously, the charge density of O²⁻ would increase with the decline of O1s binding energy, owing to the substitution of Zr⁴⁺ by Ca²⁺ and to the reduced positive charges in the resulted catalysts, which had been proved by the foregoing XRD, Raman, and XPS techniques. Consequently, more and strong basic sites were created. On the other hand, the increasing of the Ca content led to a decreased surficial area, which might in turn reduce the exposed basic sites. The positive effect caused by the addition of Ca²⁺ on their basic property was predominant when *n* was in the range of 0-0.6. However, the negative effect caused by doping of Ca²⁺ surpassed its positive influence when *n* > 0.6. Coupled with the fact that the number of weak sites was almost independent of *n* except for pure ZrO₂ (see Table 1), the change of total basic sites for these samples exhibited a typical volcanic shape, following a decreasing order: 0.6CaO-ZrO₂ > 0.4CaO-ZrO₂ > 0.8CaO-ZrO₂ > 0.2CaO-ZrO₂ > ZrO₂.

3.3. Catalytic performance

3.3.1. Reaction system for the transesterification of DMC and glycerol

For glycerol, its two terminal hydroxyl groups are more active than the middle one. After the transesterification between DMC and the terminal hydroxyl groups, the intra-molecular transesterification involving the middle hydroxyl group and the neighboring carbonyl group was facilitated. Thus, the target product GLC was manufactured with a high yield. However, when the GLC concentration was increased, the undesired product glycerol dicarbonate (GDC) would be generated via



Scheme 2. Reaction system for the reaction of DMC and glycerol.

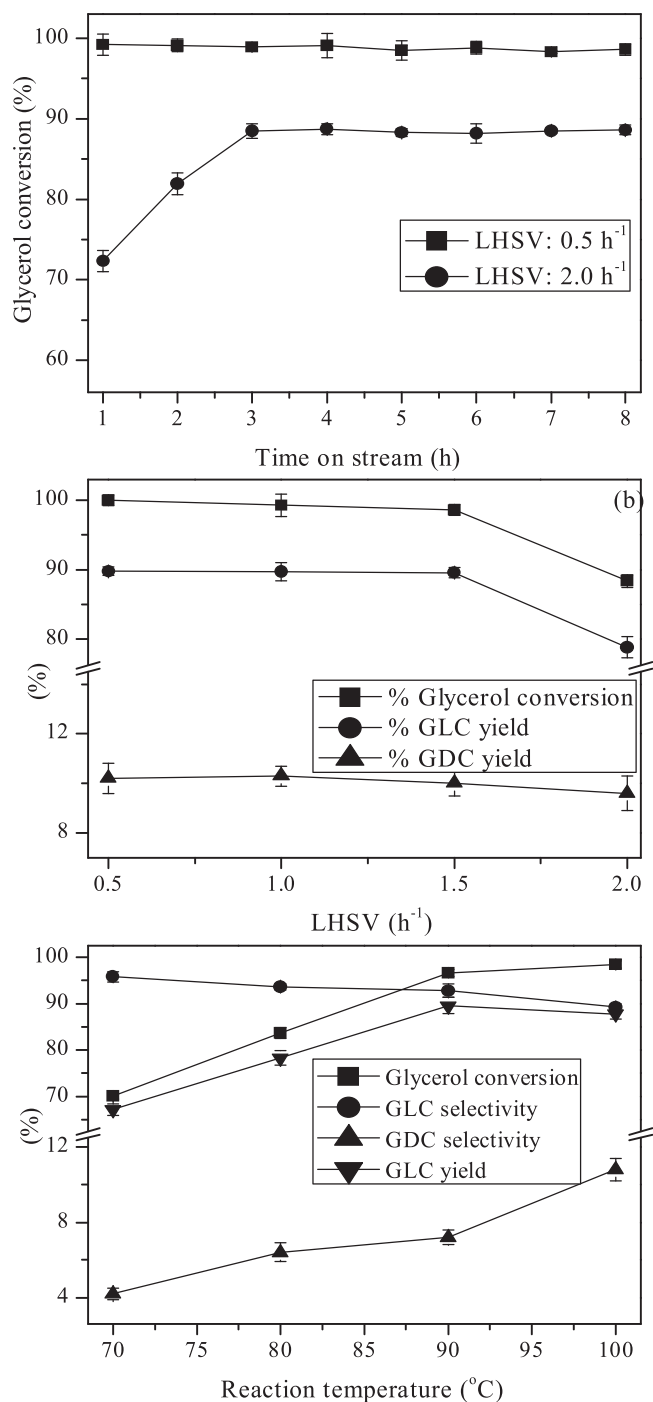


Fig. 7. Effect on reaction parameters on the GLC synthesis over 0.6CaO-ZrO₂ catalyst; error bars give the standard deviation.

Effect of diffusion (a). Reaction conditions: reaction temperature, 90 °C; catalyst, 3 mL; *n* (DMC): *n* (glycerol) = 3:1. Effect of LHSV (b). Reaction conditions: reaction temperature, 90 °C; catalyst, 3 mL; *n* (DMC): *n* (glycerol) = 3:1. Effect of reaction temperature (c). Reaction conditions: catalyst, 3 mL; *n* (DMC): *n* (glycerol) = 3:1; LHSV, 1.5 h⁻¹.

the transesterification reaction between the hydroxyl group of GLC and another DMC molecule (Scheme 2).

3.3.2. Effect of liquid hourly space velocity (LHSV)

Firstly, two different LHSV values were selected to estimate the effect of diffusion (Fig. 7(a)). Notably, the glycerol conversion increased linearly at first 2 h when the LHSV value was set at 2 h⁻¹.

Moreover, the total glycerol conversion could be obtained at a low LHSV value (0.5 h⁻¹). Apparently, the rate of this reaction was not dependent on extra-particle mass transfer. On the other hand, following these conditions, the reaction rate was calculated as 5 × 10⁻⁵ mol s⁻¹ mL⁻¹. The intra-particle diffusion degree could be evaluated using the Thiele modulus revised by Weisz [52]:

$$\phi = \frac{\nu R^2}{C_0 D_{eff}}$$

In this formula, ν is the rate of reaction (mol s⁻¹ mL⁻¹); R stands for the radius of the catalyst particle (about 0.02 cm in this work); C_0 is referred to the initial concentration of glycerol (4.3 × 10⁻⁴ mol mL⁻¹); and D_{eff} is the diffusion coefficient (selected as 10⁻⁴ cm² s⁻¹). The value of ϕ was calculated to be about 0.004, which is much less than 1.0. It was believed that the overall reaction would be restricted by diffusion when ϕ was 1.0 [52], thus, the intra-particle diffusion hardly limited the GLC synthesis in this work. In addition, the catalytic performances of ZrO₂, 0.2CaO-ZrO₂, 0.4CaO-ZrO₂ and 0.6CaO-ZrO₂ under different reaction conditions are also presented in Supplementary Material.

The effect of LHSV on the GLC production is shown in Fig. 7(b). The glycerol conversion declined slightly with an increased LHSV value from 0.5 to 1.5 h⁻¹. Nevertheless, a sharp decrease of glycerol conversion was observed when LHSV was further increased to 2.0 h⁻¹. Rationally, a higher LHSV value indicated that more reactant was employed. Considering that the catalytic ability of this 0.6CaO-ZrO₂ sample was constant, the residence time was too short for converting glycerol to GLC completely. Thus, the suitable LHSV was chosen as 1.5 h⁻¹ in this work.

3.3.3. Effect of reaction temperature

The effect of varying the temperature from 70 to 100 °C on the reaction was studied in the case of 0.6CaO-ZrO₂ (see Fig. 7(c)). The results presented that the glycerol conversion increased rapidly until 90 °C. This might be explained by the vaporization loss of co-produced methanol from reaction system, driving the reaction towards the GLC production [53]. However, higher temperatures also accelerated the rate of further reaction to generate GDC. Consequently, the GLC selectivity declined constantly with the increase of the reaction temperature. Based on these facts, the GLC yield reached its maximal value of 90% at 90 °C, but showed a slight decrease when the reaction reached at 100 °C. Therefore, the optimal reaction temperature was selected as 90 °C.

3.3.4. Effect of Ca content and basic property

The catalytic performance of various catalysts with a different Ca content after reaction of 8 h is illustrated in Fig. 8(a). Without catalyst, no significant glycerol conversion was obtained. All the Ca-containing catalysts gave higher glycerol conversion when compared to pure ZrO₂, pointing out the positive effect of Ca on the reaction. Moreover, the glycerol conversion was related highly to the value of *n*. The catalyst ZrO₂ exhibited a low reactivity of 50% glycerol conversion, while a high conversion of 78% could be achieved for the catalyst 0.8CaO-ZrO₂. Specially, the catalyst 0.6CaO-ZrO₂ reached the highest glycerol conversion of 97%. Taking into account of the enhancement of surface basicity, it seemed that the high number of basic sites could induce a high catalytic ability towards the transesterification reaction. Indeed, this hypothesis was supported by Fig. 8(a), where the sequence of glycerol conversion was consistent roughly with that of total amounts of basic sites. Similar conclusions were also drawn in previous works [24,26,28,54]. In addition, TOF values of catalysts in the kinetic regions (not at a very high glycerol conversion) are a useful clue to unravel the role of basic property to their activity; where TOF denotes as the number of glycerol molecules converted on a unit basic site per hour (h⁻¹). Thus, we demonstrate the glycerol conversion, total number of basic sites on the catalysts and TOF values for the *n*CaO-ZrO₂ at 90 °C

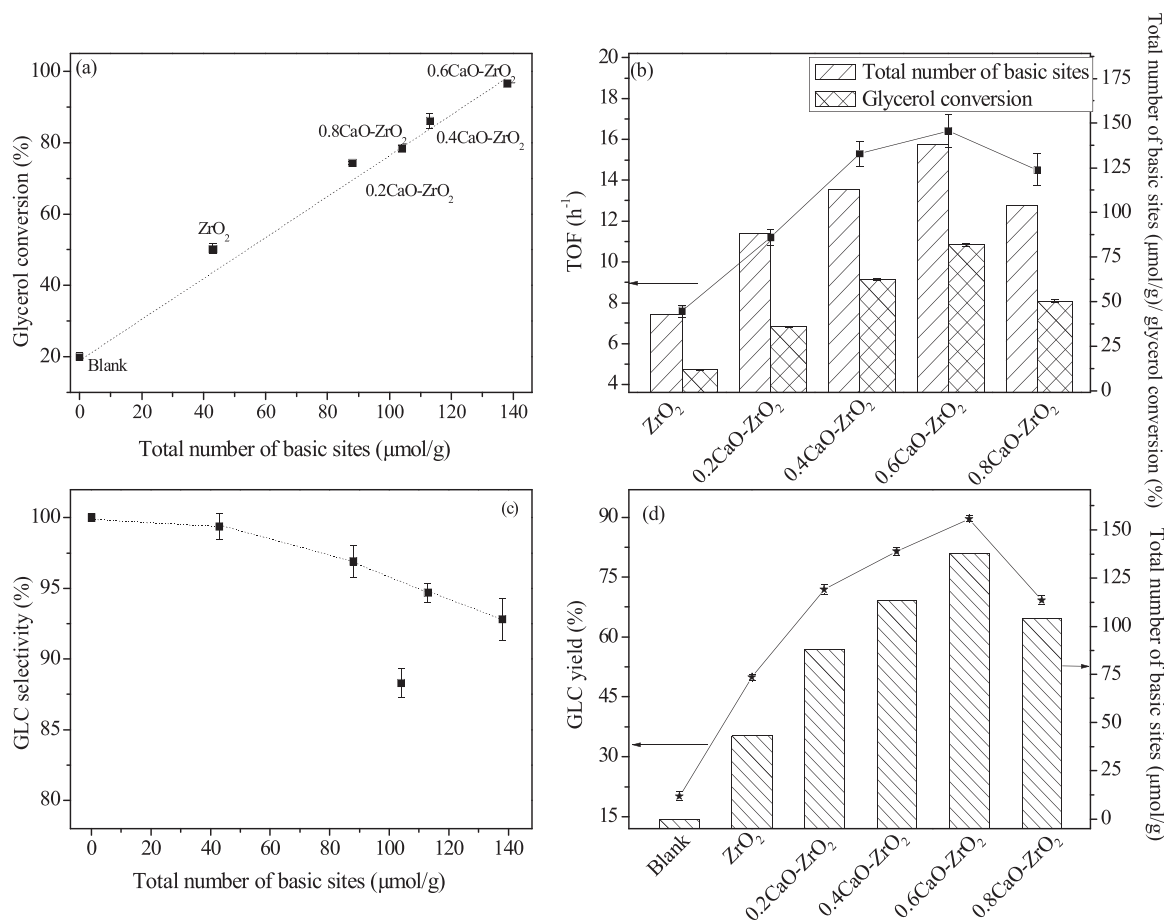


Fig. 8. Effect of Ca content and basic property on the GLC synthesis; error bars give the standard deviation.

The relationship between glycerol conversion (a); TOF values (b); GLC selectivity (c); GLC yield (d); and total number basic sites.

Reaction conditions for (a), (c) and (d): 90 °C, catalyst, 3 mL; *n* (DMC): *n* (glycerol) = 3:1; LHSV, 1.5 h⁻¹.

Reaction conditions for (b): 80 °C, catalyst, 3 mL; *n* (DMC): *n* (glycerol) = 3:1; LHSV, 2.0 h⁻¹.

with 2 h⁻¹ of LHSV in Fig. 8(b). Apparently, the TOF values of the catalysts containing Ca are higher than that of bare ZrO₂. Moreover, the TOF values presented a typical volcano-shaped profile in terms of Ca loadings and the catalyst 0.6CaO-ZrO₂ possessed the highest TOF value at 16.4 h⁻¹. This fact further highlights the importance of basic sites for samples towards the transformation of glycerol during reaction.

Aiming at further investigating the role of every basic species (weak, moderate and strong basic sites) towards the reaction of DMC between glycerol separately, all the precursors were treated at variable temperatures ranging from 200 to 600 °C. Generally, after calcination at a relatively low temperature (200 °C), the catalytic ability of mixed oxide mostly originated from weak basic sites associated with OH⁻, created by decomposition of surface bicarbonate species [55]. Upon calcination at 400 °C, only partial decomposition occurred, thus, the catalytic ability was related to both weak and moderate basic sites. In case of thorough decomposition at higher temperatures like 600 °C, the catalytic ability was ascribed to the united force of the three types of basic sites (weak OH⁻, moderate Ca/Zr-O pairs and strong O²⁻ sites) [55]. The effect of 600 °C on the catalytic performances is illustrated in Fig. 8(a), so, we only show the catalytic results of various samples that were obtained at 200 and 400 °C, respectively (see Fig S(2) in Supplementary material). When the calcination temperature was at 200 °C, the catalytic ability of samples, expressed by glycerol conversion, altered only a little except for pure ZrO₂. It might be attributed to the fact that these *n*CaO-ZrO₂ catalysts exhibited similar amounts of weak basic sites (see Table 1). Importantly, their activity order was in good agreement with that of weak basic sites density and the catalyst 0.2 CaO-ZrO₂ gave

the highest glycerol conversion of 46% (see Fig. S2(a) in Supplementary material). When the calcination temperature was at 400 °C, the catalytic ability increased in an order: 0.6CaO-ZrO₂ > 0.4CaO-ZrO₂ > 0.2CaO-ZrO₂ > 0.8CaO-ZrO₂ > ZrO₂. It was noted that this order is agreement with the variation in the number of both weak and moderate sites (see Fig. S2(b) in Supplementary Material). All these findings ascertained that the surficial basic sites of catalysts played a vital role for the transesterification reaction. In other words, each basic species might have a similar activity towards the glycerol conversion for GLC synthesis.

Fig. 8(c) shows the plot of product selectivity against the total amount of basic sites for all the catalysts. It is clearly shown that the selectivity of GLC was depressed when more basic sites were present on the surfaces of the catalysts. Correspondingly, the selectivity of by-product GDC increased with the increasing of basic density. For instance, the strongly basic catalyst 0.6CaO-ZrO₂ exhibited inferior GLC selectivity in comparison with 0.2CaO-ZrO₂. It should be noted that the catalyst 0.8CaO-ZrO₂ also showed a high reactivity for the GDC synthesis, despite that it had smaller basic density than that of 0.6CaO-ZrO₂. This might be attributed to its strong basic strength, as illustrated by the CO₂-TPD analysis. Finally, the catalytic behaviors of these materials with respect to GLC yield are illustrated in Fig. 8(d). As expected, 0.6CaO-ZrO₂ showed the superior catalytic performance than the other catalysts with a 90%-yield of GLC. This highlighted that a right basic property was vital afford a high GLC yield.

Based on the experimental results and discussion aforementioned, a plausible reaction mechanism was proposed (see Scheme 3(a)). First,

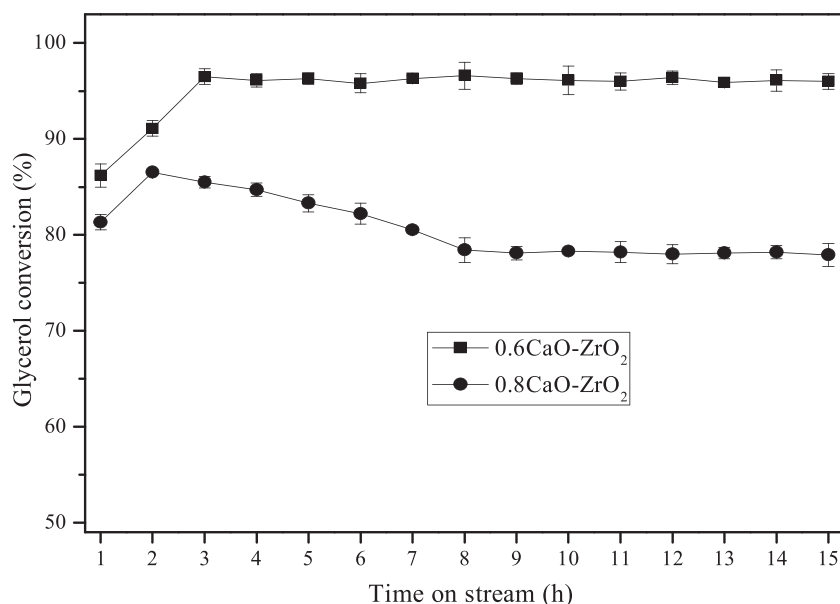


Fig. 9. Conversion of glycerol over 0.6CaO-ZrO₂ and 0.8CaO-ZrO₂ catalysts in a long-term test. Reaction reactions: 90 °C, catalyst, 3 mL; *n* (DMC): *n* (glycerol) = 3:1; LHSV, 1.5 h⁻¹. Error bars give the standard deviation.

Table 2

Catalytic behavior comparison of current 0.6CaO-ZrO₂ catalyst with other reported Ca-based catalysts.

Catalyst	Time (h)	Glycerol conversion (%)	GLC selectivity (%)	Production mode	Reference
0.6CaO-ZrO ₂	–	97	93	Continuous	Present work
0.6CaO-ZrO ₂ ^a	2	100	90	Intermittent	Present work
CaO	1.5	74.4	86.0	Intermittent	[21]
CaO	3	77	87	Intermittent	[33]
Ca-Al hydrocalumite	3	75	98	Intermittent	[32]
CaAl-layerd hydroxide	3	82	61	Intermittent	[33]
CaO-Al ₂ O ₃	3	93	97	Intermittent	[32]
CaO-MgO	1.5	100	100	Intermittent	[34]

Reaction conditions: glycerol 40 mmol, DMC 120 mmol, 0.3 g catalyst, 90 °C, 2 h.

glycerol conversion of 87% for the reaction time of 2 h from the start, the conversion decreased gradually to 78% after a reaction time of 8 h. Then, its activity remained at a certain level. As discussed above, the basic sites of the catalyst 0.6CaO-ZrO₂ mainly originated from the addition of Ca²⁺ into ZrO₂. Consequently, all the basic species were firmly anchored onto the *t*-ZrO₂ framework thanks to the formation of solid solution. These basic sites were highly dispersed in the ZrO₂ lattice, rather than that CaO simply coated on ZrO₂, which was seen for the supported bases obtained via impregnation. Therefore, the solid-solution structure endowed the nature of high structural stability for the catalyst 0.6CaO-ZrO₂. For the catalyst 0.8CaO-ZrO₂, a fraction of its basic sites stems from the separated CaO phase, and thus they are weakly bound to catalyst surface. When it was employed to catalyze GLC synthesis, this fraction of basic sites was easily lost due to the generation of dissolved Ca-species [30–32]. Moreover, the two catalysts were analyzed by elemental analysis and CO₂-TPD techniques after the reactions. The analytic results demonstrate no obvious changes for the Ca content for the catalyst 0.6CaO-ZrO₂. Nevertheless, the Ca:Zr ratio initially used in the catalyst 0.8CaO-ZrO₂ decreased to a certain extent. Furthermore, the deviation of basic concentration between fresh and used 0.6CaO-ZrO₂ (135 μmol g⁻¹) could be negligible, while the number of basic sites of used 0.8CaO-ZrO₂ (93 μmol g⁻¹) had a noticeable decline. Once the leaching of these free CaO phase terminated, the residual basic species originated from the solid solution structure would give a stable glycerol conversion with flushing of reactant.

Additionally, the used 0.6CaO-ZrO₂ catalyst after a time of 15 h in the fixed-bed was recovered by centrifuge, washed by ethanol for three

times, dried at 100 °C, and was then characterized by means of XRD and TEM (see Fig. S3 and Fig. S4 in Supplementary Material). It was found that the used catalyst still retained the solid solution structure and wormhole-like ordered mesoporous frameworks. Moreover, N₂ adsorption/desorption technique further revealed that the used catalyst possessed a high BET surface area (164 m² g⁻¹). It is thus concluded that the catalyst 0.6CaO-ZrO₂ has an excellent reusability and a good structural stability.

3.5. Activity comparisons

It is difficult to directly compare the present catalyst 0.6CaO-ZrO₂ with the reported Ca-containing catalysts since they were evaluated in a different way from the present work. Herein, we further tested catalyst 0.6CaO-ZrO₂ with a batch reactor. The typical catalytic assessment is illustrated in Supplementary Material, and the comparison results are given in Table 2. It was worth mentioning that the glycerol conversion obtained in the batch reactor was higher than that achieved in the fixed-bed, whereas the GLC selectivity showed a slight decrease with 0.6CaO-ZrO₂. The above changes might be attributed to the relatively long residual time (2 h) for reagent on catalyst in batch reactor compared to that in fixed-bed reactor. Thus, the accessibility of the reactant to the active sites was greatly enhanced. However, a long residual time also induced more probability for side reactions, reducing GLC selectivity to some extent. Despite of this negative effect, the catalyst 0.6CaO-ZrO₂ still afforded a GLC yield of 90% within a reaction of 2 h at 90 °C. Taking into account the fact that bare CaO only gave about

80% glycerol conversion [21,33], the carrier ZrO_2 was thus efficient to enhance the reactivity remarkably. Moreover, the major shortcomings like low surface area and rapid deactivation caused by CO_2 contamination hindered industrial utilization of pure CaO. Furthermore, many researchers had discovered that its activity mostly ascribed to the homogeneous Ca-species [30,31]. Other Ca-based catalysts such as Ca-Al hydrocalumite [32], Ca-Al layered double hydroxide [33], $CaO-Al_2O_3$ [32] and $CaO-MgO$ [34] possessed higher activity than that of CaO, but they suffered from the leaching of active CaO site into reaction medium, severely inhibiting their practical applications [30,31]. In addition, the comparative TOF results of the present $0.6CaO-ZrO_2$ and reported Ca-based samples are listed in Table S2 in Supplementary Material. We calculated the TOF value following the method proposed by Kumar et al. [56] (see Supplementary Material). To our delight, the catalyst $0.6CaO-ZrO_2$ gave a high TOF value of 12.2 h^{-1} , which was only inferior to $CaO-MgO$ mixed oxide. When the poor stability of $CaO-MgO$ is taken into account, the catalyst $0.6CaO-ZrO_2$ is of highly practical one for continuous and efficient production of GLC.

4. Conclusion

In this work, we have developed a method for preparations of mesoporous $CaO-ZrO_2$ solid bases via a simple surfactant-free co-precipitation procedure. The $CaO-ZrO_2$ catalysts prepared by this method possessed a uniformly mesoporous structure and a large specific surface area, which was favorable for exposure of more basic sites. Moreover, the basic density of these samples was highly related to the Ca:Zr ratio and exhibited a volcano trend with the rise of a Ca content. Importantly, after the incorporation of Ca^{2+} into ZrO_2 lattice, various characterization results proved that the basic sites were firmly dispersed in the substrate thanks to the formation of solid solution. The catalyst $0.6CaO-ZrO_2$ showed a striking activity and a good stability for the continuous synthesis of GLC in a fixed-bed reactor. Furthermore, a good correlation between the catalytic activity and the total amount of surface basic sites has been established. However, the consecutive transesterification between GLC and DMC would take place severely over basic materials with too much basic sites/strong basic strength. Among all the catalysts, $0.6CaO-ZrO_2$ showed the best catalytic performance with a 97% glycerol conversion and a 93% GLC selectivity. Thus, this work provides a new avenue for fabricating Ca-based catalyst with a good reactivity and a long durability for the continuous synthesis of GLC via transesterification between DMC and glycerol.

Acknowledgements

This work is financially supported by the Key Research and Development Program of Shandong Province (2018GGX107010), Natural Science Foundation of Shandong Province (ZR2016BL21, ZR2018LB030), Science and Technology Research Program for Colleges and Universities in Shandong Province (J18KA107), Zaozhuang independent innovation and achievements transformation projects (201502) and National Training Programs of Innovation and Entrepreneurship for Undergraduates (201710904063, 201710904064).

Appendix A. Supplementary data

Supplementary material related to this article can be found, in the online version, at doi:<https://doi.org/10.1016/j.apcata.2019.117313>.

References

[1] A. Taghizadeh-Alisaraei, H.A. Assar, B. Ghobadian, A. Motevali, *Renew. Sust. Energ. Rev.* 72 (2017) 510–522.
 [2] G.M. Lari, G. Pastore, M. Haus, Y. Ding, S. Papadokostantakis, C. Mondelli, J. Pérez-Ramírez, *Synth. Lect. Energy Environ. Technol. Sci. Soc.* 11 (2018)

1012–1029.
 [3] B. Das, K. Mohanty, *Ind. Eng. Chem. Res.* 58 (2019) 15803–15817.
 [4] Z.I. Ishak, N.A. Sairi, Y. Alias, M.K.T. Aroua, R. Yusoff, 297 (2016) 128–138.
 [5] M.O. Sonnatí, S. Amigoni, E.P. Taffin de Givenchy, T. Darmanin, O. Choulet, F. Guittard, *Green Chem.* 15 (2013) 283–306.
 [6] W. Luo, L. Sun, Y. Yang, Y. Chen, Z. Zhou, J. Liu, F. Wang, *Catal. Sci. Technol.* 8 (2018) 6468–6477.
 [7] A.-A.G. Shaikh, S. Sivaram, *Chem. Rev.* 96 (1996) 951–976.
 [8] J. Hu, Y. Gu, Z. Guan, J. Li, W. Mo, T. Li, G. Li, *ChemSusChem* 4 (2011) 1767–1772.
 [9] A.J. Kamphuis, F. Picchioni, P.P. Pescarmona, *Green Chem.* 21 (2019) 406–448.
 [10] X. Su, W. Lin, H. Cheng, C. Zhang, Y. Wang, X. Yu, Z. Wu, F. Zhao, *Green Chem.* 19 (2017) 1775–1781.
 [11] S. Dabral, T. Schaub, *Adv. Synth. Catal.* 361 (2019) 223–246.
 [12] D. Wang, X. Zhang, X. Cong, S. Liu, D. Zhou, *Appl. Catal. A Gen.* 555 (2018) 36–46.
 [13] D. Fakhraee, R.J. Chimentão, F. Medina, A. Urakawa, *ACS Catal.* 5 (2015) 6284–6295.
 [14] H. Nguyen-Phu, E.W. Shin, *J. Catal.* 373 (2019) 147–160.
 [15] P. Devi, U. Das, A.K. Dalai, *Chem. Eng. J.* 346 (2018) 477–488.
 [16] M. Marimuthu, P. Marimuthu, S. Palanivelu, V. Rajagopalan, *Mol. Catal.* 460 (2018) 53–62.
 [17] Z.I. Ishak, N.A. Sairi, Y. Alias, M.K.T. Aroua, R. Yusoff, *Catal. Rev.* 59 (2017) 44–93.
 [18] B. Liu, C. Li, G. Zhang, X. Yao, S.S.C. Chuang, Z. Li, *ACS Catal.* 8 (2018) 10446–10456.
 [19] A. Bansode, A. Urakawa, *ACS Catal.* 4 (2014) 3877–3880.
 [20] M. Tudorache, A. Negoii, V.I. Parvulescu, *Catal. Today* 279 (2017) 71–76.
 [21] J.R. Ochoa-Gómez, O. Gómez-Jiménez-Aberasturi, B. Maestro-Madurga, A. Pesquera-Rodríguez, C. Ramírez-López, L. Lorenzo-Ibarreta, J. Torrecilla-Soria, M.C. Villarín-Velasco, *Appl. Catal. A Gen.* 366 (2009) 315–324.
 [22] R. Bai, Y. Wang, S. Wang, F. Mei, T. Li, G. Li, *Fuel Process. Technol.* 106 (2013) 209–214.
 [23] J. Zhen, M. Liu, M. Kang, Ning Yin, X. Wang, Y. Tan, Y. Zhu, *J. Brazil. Chem. Soc.* 25 (2014) 152–160.
 [24] X. Song, Y. Wu, F. Cai, D. Pan, G. Xiao, *Appl. Catal. A Gen.* 532 (2017) 77–85.
 [25] S. Pan, L. Zheng, R. Nie, S. Xia, P. Chen, Z. Hou, *Chinese J. Catal.* 33 (2012) 1772–1777.
 [26] D. Singh, B. Reddy, A. Ganesh, S. Mahajani, *Ind. Eng. Chem. Res.* 53 (2014) 18786–18795.
 [27] F.S.H. Simanjuntak, V.T. Widayana, C.S. Kim, B.S. Ahn, Y.J. Kim, H. Lee, *Chem. Eng. Sci.* 94 (2013) 265–270.
 [28] G. Parameswaram, M. Srinivas, B. Hari Babu, P.S. Sai Prasad, N. Lingaiah, *Catal. Sci. Technol.* 3 (2013) 3242–3249.
 [29] X. Zhang, D. Wang, J. Ma, W. Wei, *Catal. Lett.* 147 (2017) 1181–1196.
 [30] J. Li, T. Wang, *React. Kinet. Mech. Catal.* 102 (2011) 113–126.
 [31] F.S.H. Simanjuntak, T.K. Kim, S.D. Lee, B.S. Ahn, H.S. Kim, H. Lee, *Appl. Catal. A Gen.* 401 (2011) 220–225.
 [32] L. Zheng, S. Xia, X. Lu, Z. Hou, *Chinese J. Catal.* 36 (2015) 1759–1765.
 [33] J. Granados-Reyes, P. Salagre, Y. Cesteros, *Appl. Clay Sci.* 132–133 (2016) 216–222.
 [34] M.S. Khayoon, B.H. Hameed, *Appl. Catal. A Gen.* 466 (2013) 272–281.
 [35] T. Yamaguchi, *Catal. Today* 20 (1994) 199–217.
 [36] Z. Liu, W. Zhao, F. Xiao, W. Wei, Y. Sun, *Catal. Commun.* 11 (2010) 675–678.
 [37] S. Liu, X. Zhang, J. Li, N. Zhao, W. Wei, Y. Sun, *Catal. Commun.* 9 (2008) 1527–1532.
 [38] M. Varkolu, D.R. Burri, S.R.R. Kamaraju, S.B. Jonnalagadda, W.E. Van Zyl, *J. Porous Mat.* 23 (2016) 185–193.
 [39] X. Zhang, D. Wang, G. Wu, X. Wang, X. Jiang, S. Liu, D. Zhou, D. Xu, J. Gao, *Appl. Catal. A Gen.* 555 (2018) 130–137.
 [40] J. Wang, G. Li, Z. Li, C.H. Tang, Z.H. Feng, H. An, H. Liu, T. Liu, C. Li, *Sci. Adv.* 3 (2017) e1701290.
 [41] Z.H. Ma, R. Xu, C.H. Yang, W. Wei, W. Li, Y. Sun, *Acta Phys. Chim. Sin.* 20 (2004) 1221–1225.
 [42] S. Pradhan, V. Sahu, B.G. Mishra, *J. Mol. Catal. A Chem.* 425 (2016) 297–309.
 [43] S. Figueroa, J. Desimoni, P.C. Rivas, M.M. Cervera, M.C. Caracocha, O. Sanctis, *Chem. Mater.* 17 (2005) 3486–3491.
 [44] L. Chen, J. Hu, R.M. Richards, *ChemPhysChem* 9 (2008) 1069–1078.
 [45] M.L. Granados, M.D.Z. Poves, D.M. Alonso, R. Mariscal, F.C. Galisteo, R. Moreno-Tost, J. Santamaría, J.L.G. Fierro, *Appl. Catal. B Environ.* 73 (2007) 317–326.
 [46] R. Koirala, K.R. Gunugunuri, S.E. Pratsinis, P.G. Smirniotis, *J. Phys. Chem. C* 115 (2011) 24804–24812.
 [47] S. Luz Martínez, R. Romero, J.C. López, A. Romero, V. Sánchez Mendieta, R. Natividad, *Ind. Eng. Chem. Res.* 50 (2011) 2665–2670.
 [48] M.I. Sosulnikov, Y.A. Teterin, *J. Electron Spectros. Relat. Phenomena* 59 (1992) 111–126.
 [49] F. Jiao, A. Harrison, J.-C. Jumas, A.V. Chadwick, W. Kockelmann, P.G. Bruce, *J. Am. Chem. Soc.* 128 (2006) 5468–5474.
 [50] M. Rezaei, S.M. Alavi, S. Sahebdehfar, P. Bai, X. Liu, Z.-F. Yan, *Appl. Catal. B Environ.* 77 (2008) 346–354.
 [51] Q.J. Chen, J. Zhang, Q.W. Jin, B.R. Pan, W.B. Kong, T.J. Zhao, Y.H. Sun, *Catal. Today* 215 (2013) 251–259.
 [52] P.B. Weisz, *Science* 179 (1973) 433–440.
 [53] F.S.H. Simanjuntak, J.S. Choi, G. Lee, H.J. Lee, S.D. Lee, M. Cheong, H.S. Kim, H. Lee, *Appl. Catal. B Environ.* 165 (2015) 642–650.
 [54] K. Hu, H. Wang, Y. Liu, C. Yang, *J. Ind. Eng. Chem.* 28 (2015) 334–343.
 [55] P. Liu, M. Derchi, E.J.M. Hensen, *Appl. Catal. B Environ.* 144 (2014) 135–143.
 [56] P. Kumar, P. With, V. Srivastava, R. Gläser, I. Mishra, *Ind. Eng. Chem. Res.* 54 (2015) 12543–12552.